JOURNAL OF GEOPHYSICAL RESEARCH, VOL. 115, C06024, doi:10.1029/2009JC005591, 2010

Gravity waves propagating into an ice-covered ocean: A viscoelastic model

Ruixue Wang[1,2] and Hayley H. Shen[2]

Received 22 June 2009; revised 29 January 2010; accepted 26 February 2010; published 29 June 2010.

[1] A viscoelastic model is proposed to describe the propagation of gravity waves into various types of ice cover. The ice-ocean system is modeled as a homogeneous viscoelastic fluid overlying an inviscid layer. Both layers have finite thickness. The viscosity is imagined to originate from the frazil ice or ice floes much smaller than the wavelength, and the elasticity from ice floes which are relatively large compared to the wavelength. A compact form of the dispersion relation is obtained. Under proper limiting conditions this dispersion relation can be reduced to several previously established models including the mass loading model, the viscous layer model and the thin elastic plate model. The full dispersion relation contains several propagating wave modes under the ice cover. The following two criteria are used to select the dominant wave mode: (1) wave number is the closest to the open water value and (2) attenuation rate is the least among all modes. The modes selected from those criteria coincide with the ones discussed in previous studies, which are shown to be limiting cases in small or large elasticity regimes of the present model. In the intermediate elasticity regime, however, it appears that there are three wave modes with similar wavelengths and attenuation rates. Implications of this intermediate elasticity range remain to be seen. The general viscoelastic model bridges the gap among existing models. It also provides a unified tool for wave-ice modelers to parameterize the polar regions populated with various types of ice cover.

Citation: Wang, R., and H. H. Shen (2010), Gravity waves propagating into an ice-covered ocean: A viscoelastic model, *J. Geophys. Res.*, *115*, C06024, doi:10.1029/2009JC005591.

1. Introduction

[2] Arctic sea ice is becoming more dynamic due to the drastic decline of summer sea ice extent [*Stroeve et al.*, 2008]. The resulting areas of open water now provide sufficient fetch for local winds to generate significant waves on the surface of the Arctic Ocean itself. Current sea ice models may need to incorporate wave-ice interactions to better describe the Arctic ice conditions.

[3] There have been many models developed to address how the length and height of a wave change after it enters an ice field. In general these models can be classified into two categories [*Squire*, 2007]: (1) solitary floe models based on the fact that, in principle, an ice cover consists of individual ice floes, and wave effects on large scale can be treated by a synthesis of many solitary floes and (2) continuum models in which the physical properties of the ice cover are empirically represented by certain rheological parameters. The latter will be the focus of this study. A detailed review of wave propagation through arrays of discrete floes are given by *Squire* [2007].

[1]State Key Laboratory of Structural Analysis for Industrial Equipment, Dalian University of Technology, Dalian, China.

[2]Department of Civil and Environmental Engineering, Clarkson University, Potsdam, New York, USA.

0148-0227/10/2009JC005591

[4] Several continuum models have been developed, including the mass loading model, the thin elastic plate model and the viscous layer model. Focusing on the discontinuous nature, the mass loading model considers the ice cover as a collection of noninteracting point masses [*Peters*, 1950; *Weitz and Keller*, 1950]. The resulting dispersion relation predicts wave shortening, which implies an increase of wave amplitude in the absence of any dissipative mechanism [*Wadhams and Holt*, 1991]. The thin elastic plate model assumes that sea ice behaves as a homogeneous semi-infinite thin elastic plate. It was initially developed for a continuous unbroken ice sheet [*Greenhill*, 1886]. The thin elastic plate model cannot predict attenuation, hence additional mechanisms were adopted to model the energy loss [*Wadhams*, 1973; *Squire and Allan*, 1980; *Squire*, 1984; *Liu and Mollo-Christensen*, 1988; *Squire and Fox*, 1992; *Balmforth and Craster*, 1999]. The viscous layer model considers the ice layer as a suspension of solid particles in water. This concept was first introduced by *Weber* [1987] and improved by *Keller* [1998]. The latter considered the ice cover as a viscous layer of arbitrary thickness overlying an inviscid water body. *De Carolis and Desiderio* [2002] further extended Keller's model by taking into account the viscosity of water. *De Carolis et al.* [2005] derived a theory to determine the effective viscosity of the ice slurry.

[5] There are many different types of ice cover (A. P. Worby, Observing Antarctic sea ice, CD-ROM, Antarctic

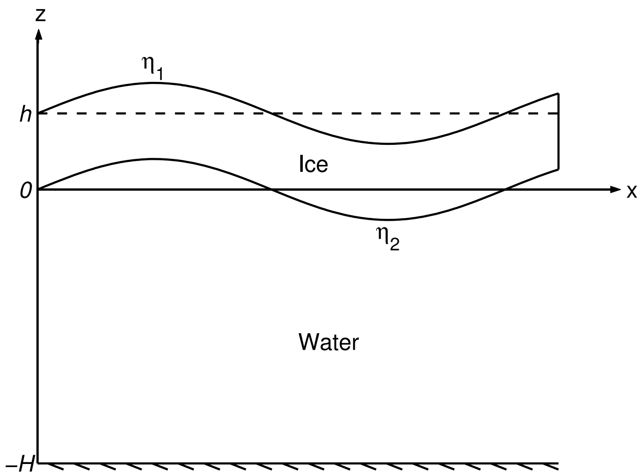

Figure 1. The sketch of the viscoelastic model.

Sea Ice Processes and Climate, Hobart, Tasmania, Australia, 1999, available at http://www.aspect.aq/cdrom.html). Near the open water, the ice cover is often made of small floes. These can either be formed from broken pack ice, as in a classic summer marginal ice zone (MIZ) or from pancakes, as found at the winter Antarctic ice edge. Both can be interspersed with frazil, or grease ice, depending on the freezing conditions. The floe size increases gradually further into the ice cover [*Squire and Moore*, 1980; *Shen et al.*, 2001; *Lu et al.*, 2008]. Eventually the cover becomes a continuous sheet, populated with ridges and leads. Currently there is no comprehensive model which can describe the propagation of gravity waves into all types of ice cover. The mass loading model failed to explain the dispersion relation observed in a laboratory test for high frequency waves in grease ice [*Newyear and Martin*, 1997]. It also overestimated the thickness of a pancake ice cover in the field [*Wadhams et al.*, 2002]. The viscous layer model, on the other hand, compared well with laboratory data of wave attenuation and dispersion in grease ice [*Newyear and Martin*, 1999]. It also appeared to be consistent with observations from a pancake ice field in the Southern Ocean [*Wadhams et al.*, 2004]. The thin elastic plate model was developed to describe a continuous ice sheet and hence is most applicable in the interior of the ice field. Some predictions from the thin elastic plate model agreed with field observations of the heavily compact ice cover near the ice edge [*Liu et al.*, 1991a, 1991b]. However, it is hard to believe it can represent the entire ice cover regardless of its composition [*Squire*, 1993, 2007].

[6] Ice thickness is difficult to measure on a large scale. The dispersion relation provides an alternative way to remotely sense the ice thickness over long distances. Using the thin elastic plate model, *Wadhams and Doble* [2009] demonstrated the ability to track the mean Arctic sea ice thickness using infragravity waves. While the Arctic Basin as a whole might be approximated as a thin elastic plate relative to infragravity waves, in smaller geophysical scales and especially wind generated waves, it is very likely different rheological models would be required to describe different ice covers. Since dispersion relations depend on the rheological models used, it is thus important to select a model that accurately reflects the type of ice present.

[7] In this paper we propose a finite thickness viscoelastic model, in which the ice layer is assumed to be a homogeneous incompressible viscoelastic fluid and the water layer is regarded as an ideal fluid. The viscosity property comes from the frazil ice or ice floes much smaller than wavelength. Interaction of these small "particles" and their hydrodynamic interaction with the surrounding water create an effective viscosity for the ice layer. The elasticity property comes from the rigidity of ice floes in which floe sizes are relatively large compared to the wavelength. When the ice is consisted of frazil or small ice floes, a viscous parameterization should be appropriate for the ice cover. When the ice cover is a continuous ice sheet, an elastic parameterization is appropriate. To describe the entire ice cover and provide a smooth transition from ice edge to its interior, a viscoelastic model may be required. The paper is organized as follows. The formulation of the viscoelastic dispersion relation is given in section 2. In section 3 the conditions for reducing the viscoelastic model to several previous models are derived. In section 4 we present the mode behavior of the viscoelastic model and compare the results with other models. The discussion and conclusion are given in sections 5 and 6 respectively.

2. Formulation

2.1. Governing Equations

[8] We consider a two-layer system in which a homogeneous viscoelastic ice layer of finite thickness h overlays an inviscid water layer of finite depth H. A two-dimensional Cartesian coordinate (O, x, z) is introduced, in which the origin is at the unperturbed interface between the two layers. The x axis is along the wave propagation direction and the z axis is upward, as shown in Figure 1. η_1 and η_2 represent the free surface and interface profiles, respectively. Considering a simple harmonic small-amplitude wave, with period T and a complex wave number k propagating in the x direction, η_1 and η_2 can be described as

$$\eta_1 = a_1 e^{i(kx-\sigma t)}, \tag{1}$$

$$\eta_2 = a_2 e^{i(kx-\sigma t)}, \tag{2}$$

where $i = \sqrt{-1}$; a is the wave amplitude and $\sigma = 2\pi/T$ is the angular frequency, t is time. Subscript 1 and 2 refer to the ice layer and water layer respectively. The complex wave number k is defined as

$$k = k_n + iq, \tag{3}$$

where the real part k_n is the wave number and the imaginary part q represents the attenuation rate.

[9] There are many ways to describe the coupling of viscosity and elasticity such as the Maxwell model, the Voigt model or various combinations of these two. There is no evidence for which one to better describe the physical properties of all types of ice cover. We shall adopt the Voigt model for simplicity, since it has been shown that the analysis for this type of viscoelastic medium can be per-

formed in the same manner as that for a pure viscous fluid by introducing a complex viscosity [*Macpherson*, 1980; *Ng and Zhang*, 2007].

[10] Using the Voigt model, the constitutive equation for a homogeneous incompressible viscoelastic medium can be described as

$$\tau_{mn} = -P_1\delta_{mn} + 2GS_{mn} + 2\rho_1\nu\dot{S}_{mn}, \tag{4}$$

where ρ_1 is the density of the ice layer; τ_{mn}, S_{mn} and $\dot{S}_{mn}$ represent the stress tensor, the strain tensor and the strain rate tensor, respectively; m and n represent x or z. G and ν are the effective shear modulus and the effective kinematic viscosity of the ice layer, respectively; P_1 is the pressure and δ_{mn} the Kronecker delta. By assuming a simple harmonic wave, the strain S_{mn} and strain rate $\dot{S}_{mn}$ can be related to each other by

$$\dot{S}_{mn} = -i\sigma S_{mn}. \tag{5}$$

The constitutive equation (4) can be simplified as

$$\tau_{mn} = -P_1\delta_{mn} + 2\rho_1\nu_e\dot{S}_{mn}, \tag{6}$$

where ν_e is the complex equivalent kinematic viscosity written as

$$\nu_e = \nu + iG/\rho_1\sigma. \tag{7}$$

The imaginary part $G/\rho_1\sigma$ measures the elasticity.

[11] The Lagrangian equations of motion for an incompressible ice layer are then given, in the linear regime, by

$$\frac{\partial \mathbf{U}_1}{\partial t} = -\frac{1}{\rho_1}\nabla P_1 + \nu_e\nabla^2\mathbf{U}_1 + \mathbf{g}, \qquad 0 \le z \le h, \tag{8}$$

where $\mathbf{U}_1$ denotes the velocity field in the ice layer and its components are u_1 and w_1. $\mathbf{g}$ is the gravitational acceleration. The continuity equation is

$$\nabla \cdot \mathbf{U}_1 = 0. \tag{9}$$

The velocity $\mathbf{U}_1$ can be split into an irrotational component and a rotational component by introducing a velocity potential ϕ_1 and a stream function ψ_1 [*Lamb*, 1932]. The velocity field in component form can be written as

$$u_1 = -\frac{\partial\phi_1}{\partial x} - \frac{\partial\psi_1}{\partial z}, \; w_1 = -\frac{\partial\phi_1}{\partial z} + \frac{\partial\psi_1}{\partial x}. \tag{10}$$

The potential and stream functions satisfy the following equations:

$$\nabla^2\phi_1 = 0, \tag{11}$$

$$\frac{\partial\psi_1}{\partial t} = \nu_e\nabla^2\psi_1, \tag{12}$$

$$\frac{\partial\phi_1}{\partial t} - \frac{P_1}{\rho_1} + \varphi = 0, \tag{13}$$

where φ is the gravitational potential.

[12] For the water layer, which is assumed to be inviscid, the equations of motion are

$$\frac{\partial \mathbf{U}_2}{\partial t} = -\frac{1}{\rho_2}\nabla P_2 + \mathbf{g}, \qquad -H \le z \le 0, \tag{14}$$

where $\mathbf{U}_2$ is the velocity field in the water layer and it components are u_2 and w_2. We can introduce a velocity potential ϕ_2 such that

$$u_2 = -\frac{\partial\phi_2}{\partial x}, \; w_2 = -\frac{\partial\phi_2}{\partial z}. \tag{15}$$

This potential satisfies

$$\nabla^2\phi_2 = 0, \tag{16}$$

$$\frac{\partial\phi_2}{\partial t} - \frac{P_2}{\rho_2} + \varphi = 0. \tag{17}$$

2.2. Boundary Conditions

[13] At the free surface, the linearized conditions of no shear stress and no normal stress are

$$\tau^1_{xz} = \rho_1\nu_e\left(\frac{\partial u_1}{\partial z} + \frac{\partial w_1}{\partial x}\right) = 0, \qquad z = h, \tag{18}$$

$$\tau^1_{zz} = -P_1 + 2\rho_1\nu_e\frac{\partial w_1}{\partial z} = 0, \qquad z = h. \tag{19}$$

The linearized kinematic condition at the free surface is given by

$$w_1 = -\frac{\partial\phi_1}{\partial z} + \frac{\partial\psi_1}{\partial x} = \frac{\partial\eta_1}{\partial t}, \qquad z = h. \tag{20}$$

The dynamic condition at the interface requires that the normal stress must be continuous, so that

$$-P_1 + 2\rho_1\nu_e\frac{\partial w_1}{\partial z} = -P_2, \qquad z = 0. \tag{21}$$

The shear stress at the interface must also be continuous. Since water is assumed to be inviscid, this shear stress at the interface vanishes

$$\tau^1_{xz} = \rho_1\nu_e\left(\frac{\partial u_1}{\partial z} + \frac{\partial w_1}{\partial x}\right) = 0, \qquad z = 0. \tag{22}$$

The continuity of normal velocity at the interface is dictated by the requirement that the two layers stay in contact. The discontinuity of the horizontal velocity is however permitted, since the water layer is assumed to be an ideal fluid. This condition can be written as

$$w_1 = w_2 = \frac{\partial\eta_2}{\partial t}, \qquad z = 0. \tag{23}$$

At the rigid bottom the vertical velocity must vanish which gives

$$w_2 = 0, \qquad z = -H. \tag{24}$$

Equations (18) and (22) can be written in terms of ϕ_1 and ψ_1 as

$$-2\frac{\partial^2\phi_1}{\partial x\partial z} - \frac{\partial^2\psi_1}{\partial z^2} + \frac{\partial^2\psi_1}{\partial x^2} = 0, \qquad z = h, \tag{25}$$

$$-2\frac{\partial^2\phi_1}{\partial x\partial z}-\frac{\partial^2\psi_1}{\partial z^2}+\frac{\partial^2\psi_1}{\partial x^2}=0, \qquad z=0. \tag{26}$$

Substituting P_1, solved from (13), into (19) gives

$$-\frac{\partial\phi_1}{\partial t}+g(h+\eta_1)+2\nu_e\left(-\frac{\partial^2\phi_1}{\partial z^2}+\frac{\partial^2\psi_1}{\partial x\partial z}\right)=0, \quad z=h. \tag{27}$$

Combining the time derivative of (27) and the kinematic condition (20), gives the linearized dynamic condition in terms of ϕ_1 and ψ_1

$$-\frac{\partial^2\phi_1}{\partial t^2}+g\left(-\frac{\partial\phi_1}{\partial z}+\frac{\partial\psi_1}{\partial x}\right)+2\nu_e\left(-\frac{\partial^3\phi_1}{\partial z^2\partial t}+\frac{\partial^3\psi_1}{\partial x\partial z\partial t}\right)=0,$$
$$z=h. \tag{28}$$

Substituting P_1 and P_2 solved from (13) and (17), respectively, into (21) yields

$$\rho_1\left(-\frac{\partial\phi_1}{\partial t}+g\eta_2\right)+2\rho_1\nu_e\frac{\partial w_1}{\partial z}=\rho_2\left(-\frac{\partial\phi_2}{\partial t}+g\eta_2\right), \qquad z=0. \tag{29}$$

Combining the time derivative of (29) and (23), gives the dynamic condition at the interface in terms of ϕ_1, ψ_1 and ϕ_2

$$\left(\frac{\rho_2}{\rho_1}-1\right)g\left(-\frac{\partial\phi_1}{\partial z}+\frac{\partial\psi_1}{\partial x}\right)$$
$$=\frac{\rho_2}{\rho_1}\frac{\partial^2\phi_2}{\partial t^2}-\frac{\partial^2\phi_1}{\partial t^2}+2\nu_e\left(-\frac{\partial^3\phi_1}{\partial z^2\partial t}+\frac{\partial^3\psi_1}{\partial x\partial z\partial t}\right), \quad z=0. \tag{30}$$

2.3. Dispersion Relation

[14] The general solution for (11) and (12) can be taken as

$$\phi_1(x,z,t)=(A\cosh kz+B\sinh kz)e^{i(kx-\sigma t)}, \tag{31}$$

$$\psi_1(x,z,t)=(C\cosh \alpha z+D\sinh \alpha z)e^{i(kx-\sigma t)}, \tag{32}$$

where $\alpha^2 = k^2 - i\sigma/\nu_e$. The general solution for (16) can be taken as

$$\phi_2(x,z,t)=E\cosh k(z+H)e^{i(kx-\sigma t)}, \tag{33}$$

which satisfies the rigid bottom boundary condition (24). By noting that

$$\frac{\partial^2\phi_2}{\partial t^2}=\frac{i\sigma}{k\tanh k(z+H)}\left(-\frac{\partial^2\phi_1}{\partial z\partial t}+\frac{\partial^2\psi_1}{\partial x\partial t}\right), \quad z=0. \tag{34}$$

Equation (30) becomes

$$\left(\frac{\rho_2}{\rho_1}-1\right)g\left(-\frac{\partial\phi_1}{\partial z}+\frac{\partial\psi_1}{\partial x}\right)-\frac{\rho_2}{\rho_1}\frac{i\sigma}{k\tanh k(z+H)}\left(-\frac{\partial^2\phi_1}{\partial z\partial t}+\frac{\partial^2\psi_1}{\partial x\partial t}\right)$$
$$+\frac{\partial^2\phi_1}{\partial t^2}-2\nu_e\left(-\frac{\partial^3\phi_1}{\partial z^2\partial t}+\frac{\partial^3\psi_1}{\partial x\partial z\partial t}\right)=0, \quad z=0. \tag{35}$$

Substituting (31), (32) and (33) into (25), (26), (28) and (35), gives

$$2ik^2B+(\alpha^2+k^2)C=0, \tag{36}$$

$$2ik^2(A\sinh kh+B\cosh kh)+(\alpha^2+k^2)(C\cosh\alpha h+D\sinh\alpha h)=0, \tag{37}$$

$$A(N\sigma\cosh kh-gk\sinh kh)+B(N\sigma\sinh kh-gk\cosh kh)$$
$$+C(igk\cosh\alpha h+2k\alpha\sigma\nu_e\sinh\alpha h)$$
$$+D(igk\sinh\alpha h+2k\alpha\sigma\nu_e\cosh\alpha h)=0, \tag{38}$$

$$N\sigma A+MB-iMC+2k\alpha\sigma\nu_e D=0, \tag{39}$$

where

$$N=\sigma+2ik^2\nu_e, \tag{40}$$

$$M=\left(\frac{\rho_2}{\rho_1}-1\right)gk-\frac{\rho_2}{\rho_1}\frac{\sigma^2}{\tanh kH}. \tag{41}$$

The dispersion relation relating σ and k can be obtained by imposing that the determinant of the coefficients of the system of equations (36)–(39) vanishes. Hence, after some algebraic manipulations, the dispersion relation is obtained as

$$\sigma^2=Q_c gk\tanh kH, \tag{42}$$

where

$$Q_c=1+\frac{\rho_1}{\rho_2}\cdot\frac{g^2k^2S_kS_\alpha-(N^4+16k^6\alpha^2\nu_e^4)S_kS_\alpha-8k^3\alpha\nu_e^2N^2(C_\alpha C_k-1)}{gk(4k^3\alpha\nu_e^2S_kC_\alpha+N^2S_\alpha C_k-gkS_kS_\alpha)} \tag{43}$$

is the modification coefficient induced by ice layer to the dispersion relation for open water. In (43), $S_k = \sinh kh$, $S_\alpha = \sinh \alpha h$, $C_k = \cosh kh$, $C_\alpha = \cosh \alpha h$.

[15] Defining $\tilde{k} = kh$, $\tilde{H} = Hh^{-1}$, $\tilde{\sigma} = \sigma(h/g)^{1/2}$, $\tilde{\alpha} = \alpha h$, $\tilde{\nu}_e = \nu_e(gh^3)^{-1/2}$, $\rho = \rho_1/\rho_2$, the dimensionless dispersion relation is obtained

$$\tilde{\sigma}^2=\tilde{Q}_c\tilde{k}\tanh\tilde{k}\tilde{H}, \tag{44}$$

where

$$\tilde{Q}_c=1+\rho\frac{\tilde{k}^2S_{\tilde{k}}S_{\tilde{\alpha}}-(\tilde{N}^4+16\tilde{k}^6\tilde{\alpha}^2\tilde{\nu}_e^4)S_{\tilde{k}}S_{\tilde{\alpha}}-8\tilde{k}^3\tilde{\alpha}\tilde{\nu}_e^2\tilde{N}^2(C_{\tilde{\alpha}}C_{\tilde{k}}-1)}{4\tilde{k}^4\tilde{\alpha}\tilde{\nu}_e^2S_{\tilde{k}}C_{\tilde{\alpha}}+\tilde{k}\tilde{N}^2S_{\tilde{\alpha}}C_{\tilde{k}}-\tilde{k}^2S_{\tilde{k}}S_{\tilde{\alpha}}} \tag{45}$$

and $S_{\tilde{k}} = \sinh\tilde{k}$, $S_{\tilde{\alpha}} = \sinh\tilde{\alpha}$, $C_{\tilde{k}} = \cosh\tilde{k}$, $C_{\tilde{\alpha}} = \cosh\tilde{\alpha}$, $\tilde{N} = \tilde{\sigma} + 2i\tilde{k}^2\tilde{\nu}_e$.

3. Special Cases

[16] Under proper conditions, the dispersion relation (44) can be reduced to several previously developed models, namely the mass loading model, the thin elastic plate model and the viscous layer model.

3.1. Mass Loading Model

[17] The ice layer is assumed to be noninteracting in the mass loading model. Hence, we take the normalized com-

plex equivalent kinematic viscosity $\tilde{\nu}_e$ to be zero. The dispersion relation (44) becomes

$$\frac{\tilde{\sigma}^2}{\tilde{k}\tanh\tilde{k}\tilde{H}} = 1 + \rho\frac{\tilde{k}^2 S_{\tilde{k}} - \tilde{\sigma}^4 S_{\tilde{k}}}{\tilde{k}\tilde{\sigma}^2 C_{\tilde{k}} - \tilde{k}^2 S_{\tilde{k}}}, \tag{46}$$

which is the dispersion relation for the two inviscid layers model [*Lamb*, 1932, p. 372]. If we further assume the wavelength to be long compared to the ice thickness, i.e., $\tilde{k} \ll 1$, then $\tanh \tilde{k} \approx \tilde{k}$ and the dispersion relation becomes

$$\tilde{\sigma}^4(1 + \rho\tilde{k}\tanh\tilde{k}\tilde{H}) - \tilde{\sigma}^2\tilde{k}\tanh\tilde{k}\tilde{H} - \tilde{\sigma}^2\tilde{k}^2 + (1-\rho)\tilde{k}^3\tanh\tilde{k}\tilde{H} = 0. \tag{47}$$

By dropping higher order terms $\tilde{\sigma}^2\tilde{k}^2$ and $(1-\rho)\tilde{k}^3 \tanh \tilde{k}\tilde{H}$ in (47), the dispersion relation can be reduced to the mass loading model written as

$$\tilde{\sigma}^2(1 + \rho\tilde{k}\tanh\tilde{k}\tilde{H}) = \tilde{k}\tanh\tilde{k}\tilde{H}. \tag{48}$$

This shows that the mass loading model is the first order approximation of the two inviscid layers model with the assumption that the wavelength is long compared to the ice thickness.

3.2. Elastic Plate Model

[18] If the viscosity of ice layer is taken to be zero, then $\tilde{\nu}_e = i\tilde{G}/\rho\tilde{\sigma}$ and $\tilde{\alpha} = (\tilde{k}^2 - \rho\tilde{\sigma}^2/\tilde{G})^{1/2}$, where $\tilde{G} = G/\rho_2 gh$. The dispersion relation (44) becomes

$$\begin{aligned}\left(\frac{\tilde{\sigma}^2}{\tilde{k}\tanh\tilde{k}\tilde{H}} - 1\right)\frac{\tilde{R}^2}{\tilde{G}}&\left[-4\tilde{k}^4\tilde{\alpha}S_{\tilde{k}}C_{\tilde{\alpha}} + \tilde{k}(2\tilde{k}^2 - \tilde{R}^2)^2 S_{\tilde{\alpha}}C_{\tilde{k}} - \frac{\tilde{R}^4}{\tilde{\sigma}^2}\tilde{k}^2 S_{\tilde{k}}S_{\tilde{\alpha}}\right]\\ &= -\left[(2\tilde{k}^2 - \tilde{R}^2)^4 + 16\tilde{k}^6(\tilde{k}^2 - \tilde{R}^2)\right]S_{\tilde{k}}S_{\tilde{\alpha}}\\ &\quad + 8\tilde{k}^3\tilde{\alpha}(2\tilde{k}^2 - \tilde{R}^2)^2(C_{\tilde{\alpha}}C_{\tilde{k}} - 1) + \frac{\tilde{R}^8}{\tilde{\sigma}^4}\tilde{k}^2 S_{\tilde{k}}S_{\tilde{\alpha}},\end{aligned} \tag{49}$$

where $\tilde{R}^2 = \rho\tilde{\sigma}^2/\tilde{G}$. This is the elastic plate model with finite ice thickness. If $\tilde{R}^2 \ll \tilde{k}^2$, $\tilde{\alpha}$ can be expanded in powers of $\tilde{R}$

$$\tilde{\alpha} = \tilde{k} - \frac{\tilde{R}^2}{2\tilde{k}} - \frac{\tilde{R}^4}{8\tilde{k}^3} - \frac{\tilde{R}^6}{16\tilde{k}^5} + O(\tilde{R}^8). \tag{50}$$

Then

$$S_{\tilde{\alpha}} = S_{\tilde{k}}\left(1 + \frac{\tilde{R}^4}{8\tilde{k}^2} + \frac{\tilde{R}^6}{16\tilde{k}^4}\right) - \frac{C_{\tilde{k}}}{\tilde{k}}\left(\frac{\tilde{R}^2}{2} + \frac{\tilde{R}^4}{8\tilde{k}^2} + \frac{\tilde{R}^6}{16\tilde{k}^4}\right), \tag{51}$$

$$C_{\tilde{\alpha}} = C_{\tilde{k}}\left(1 + \frac{\tilde{R}^4}{8\tilde{k}^2} + \frac{\tilde{R}^6}{16\tilde{k}^4}\right) - \frac{S_{\tilde{k}}}{\tilde{k}}\left(\frac{\tilde{R}^2}{2} + \frac{\tilde{R}^4}{8\tilde{k}^2} + \frac{\tilde{R}^6}{16\tilde{k}^4}\right). \tag{52}$$

Substituting (50), (51) and (52) into (49) and dropping higher order terms, (49) becomes

$$\begin{aligned}&-4\tilde{k}^2 S_{\tilde{k}}^2 + 4\tilde{k}^4 - \frac{\tilde{R}^2}{\rho\tilde{\sigma}^2}\left(2\tilde{k}S_{\tilde{k}}C_{\tilde{k}} + 2\tilde{k}^2\right) + \tilde{R}^2\left(6S_{\tilde{k}}^2 + 2\tilde{k}S_{\tilde{k}}C_{\tilde{k}} - 4\tilde{k}^2\right)\\ &+ \frac{\tilde{R}^2}{\rho\tanh(\tilde{k}\tilde{H})}\left(2S_{\tilde{k}}C_{\tilde{k}} + 2\tilde{k}\right) = 0.\end{aligned} \tag{53}$$

If $\tilde{k} \ll 1$ is further assumed, $S_{\tilde{k}} \approx \tilde{k} + \tilde{k}^3/6$, $C_{\tilde{k}} \approx 1 + \tilde{k}^2/2$. The leading order equation for (53) is given as

$$\tilde{\sigma}^2 = \frac{\left(\frac{\tilde{G}}{3}\tilde{k}^4 + 1\right)\tilde{k}\tanh\tilde{k}\tilde{H}}{1 + \rho\tilde{k}\tanh\tilde{k}\tilde{H}}. \tag{54}$$

The above is the same as the dispersion relation from the thin elastic plate model for incompressible media. However, $\tilde{G}$ can be expressed by $\tilde{G} = 6\tilde{L}(1 - \upsilon)/h^3$ without loss of generality, where $\tilde{L}$ is the dimensionless flexural rigidity and υ the Poisson's Ratio. Therefore, to recover the thin elastic plate model, two conditions should be satisfied, which are given by

$$\left.\begin{aligned}\tilde{k} &\ll 1\\ \tilde{R}^2 &\ll \tilde{k}^2\end{aligned}\right\}. \tag{55}$$

Strathdee et al. [1989], in their study of moving loads across a finite thickness plate, obtained similar results as (49) and (55) using the Green's function method, without the assumption of incompressible media.

3.3. Viscous Layer Model

[19] For the case when the ice layer has no rigidity, i.e., $G = 0$, replacing $\tilde{\nu}_e$ by $\tilde{\nu}$, the dispersion relation (44) becomes identical with equation (19) of *Keller* [1998]. For the typical case in the field, where waves are long compared with ice thickness, i.e., $\tilde{k} \ll 1$, we further assume $\tilde{\sigma}/\tilde{\nu} \ll 1$ which follows that $\tilde{\alpha} = \sqrt{\tilde{k}^2 - i\tilde{\sigma}/\tilde{\nu}} \ll 1$. The asymptotic forms of the hyperbolic functions in (44) can be expressed as

$$S_{\tilde{k}} \approx \tilde{k}, \quad S_{\tilde{\alpha}} \approx \tilde{\alpha}, \quad C_{\tilde{k}} \approx 1 + \tilde{k}^2/2, \quad C_{\tilde{\alpha}} \approx 1 + \tilde{\alpha}^2/2. \tag{56}$$

Then the simplified dispersion relation can be written as

$$\frac{\tilde{\sigma}^2}{\tilde{k}\tanh\tilde{k}\tilde{H}} = 1 - \rho\frac{\tilde{\sigma}^2(\tilde{\sigma}^2 + 4i\tilde{k}^2\tilde{\sigma}\tilde{\nu}) - \tilde{k}^2}{\tilde{\sigma}^2 + 4i\tilde{k}^2\tilde{\sigma}\tilde{\nu} - \tilde{k}^2}, \tag{57}$$

which is the same as equation (29) of Keller's model. For $\tilde{k} \ll 1$, if the viscosity is assumed to be small, i.e., $\tilde{\sigma}/\tilde{\nu} \gg 1$ and $\tilde{\alpha} \gg 1$. By assuming $\tanh \tilde{\alpha} \approx 1$ and $\tanh \tilde{k} \approx \tilde{k}$, and dropping higher order terms, (44) can be simplified to (48) which is the dispersion relation from the mass loading model. This result is expected since under the current limit the ice layer is almost inviscid. Further discussion about the viscous layer model are given by *Keller* [1998] and *De Carolis and Desiderio* [2002].

4. Results of the Dispersion Relation

[20] The dispersion relation (42) is complicated and nonlinear. Typically for each set of parameters σ, h, H, G and ν, there are infinitely many values of k that satisfy the equation. Muller's method, which is a generalized secant method and is advantageous for finding complex roots [*Press et al.*, 1992], is used to solve the dispersion relation. Three initial guesses required in Muller's method are obtained from the contours of the modulus of $\tilde{\sigma}^2 - \tilde{Q}_c\tilde{k}\tanh\tilde{k}\tilde{H}$ in the complex k plane. An example of these contours is shown in Figure 2, in which the real axis represents the wave number and the imaginary axis represents the attenuation rate. Figure 2 shows

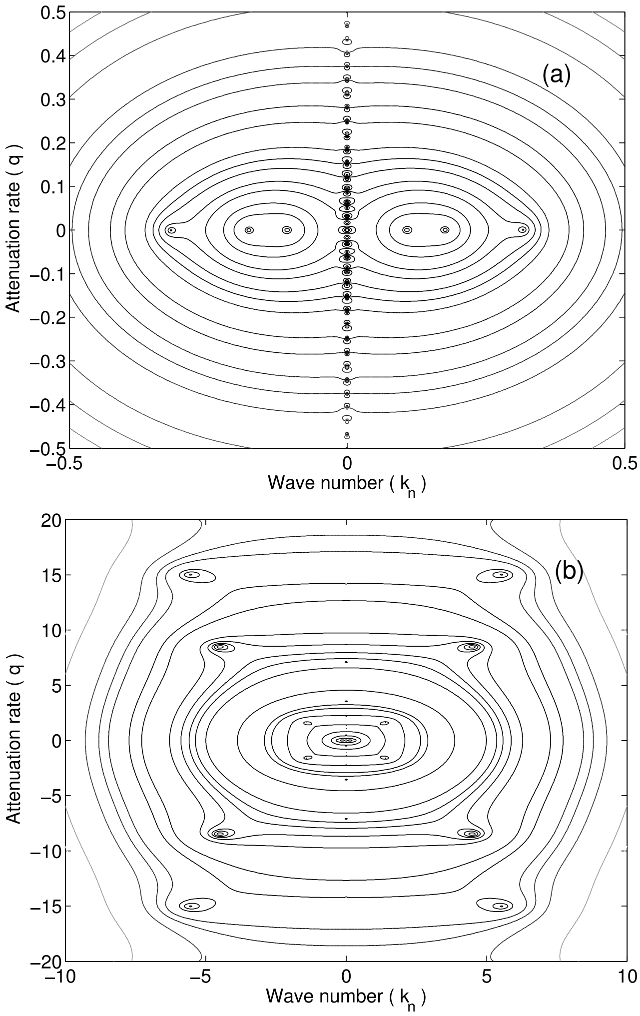

Figure 2. A typical contour plot showing the position of the various roots: (a) close-up view and (b) wide-angle view. Notice that details of the roots near the origin are lost in the wide-angle view. There are six roots shown in Figure 2a and twelve are visible in Figure 2b. Parameters used are as follows: $h = 0.5\ m$, $H = 100\ m$, $\nu = 5 \times 10^{-2}\ m^2\ s^{-1}$, $T = 6\ s$, $G = 10^4\ Pa$.

that there are an infinite number of roots slightly rotated from the imaginary axis and eighteen other complex roots in the plotted domain. Since we are interested in the progressive wave components, we shall only discuss the wave modes with a positive wave number. The wave modes with negative attenuation rates are also rejected because waves growing with distance are physically unacceptable in our study.

[21] It is shown that a single open water wave can split into many wave modes when it propagates into the ice-covered ocean. All modes share the progressive wave energy and propagate with different wave speed. Of all these waves we shall choose only one wave mode which is assumed to be the dominant one based on two criteria: (1) wave number is closest to the open water value k_0 and (2) attenuation rate is the least among all modes. The wave modes with larger wave attenuation rate dissipate rapidly, therefore they are not observable in the large scale. The wave modes with wave numbers far from k_0 are also rejected because it is assumed that most of the wave energy will be carried by the wave mode which does not alter the wave speed too much. These two criteria have been used implicitly by many [*Keller*, 1998; *Newyear and Martin*, 1999; *De Carolis and Desiderio*, 2002; *Wadhams et al.*, 2004], although they were not stated in their papers.

[22] The values of viscosity of a grease ice cover and a frazil-pancake ice field have been estimated from laboratory and field data, respectively, to be in the order of $10^{-2}\ m^2\ s^{-1}$ [*Newyear and Martin*, 1999; *Wadhams et al.*, 2004]. The typical order of magnitude of elasticity for a continuous ice plate is about $10^9\ Pa$. Based on these data we will confine our study in the range where the viscosity parameter is 0–1 $m^2\ s^{-1}$ and the elasticity parameter is 0–$10^9\ Pa$. The density ratio $\rho = 0.917$ will be used in all cases. The normalized wave number $\kappa = k_n/k_0$ is introduced for convenience. When $\kappa > 1$ the wavelength is shorter than the open water case, and $\kappa < 1$ indicates the opposite.

4.1. Two Inviscid Layers Model and Mass Loading Model

[23] As discussed in section 3, when both viscosity and elasticity are ignored, the viscoelastic model reduces to the two inviscid layers model. There are two types of propagating wave mode for the dispersion relation of the two inviscid layers model [*Lamb*, 1932; *Macpherson*, 1980]. It is known that one of the wave modes corresponds to the wave in which the free surface and the interface propagate exactly in phase, called the 'external' wave. The other corresponds to the wave mode in which the free surface and interface propagate exactly out of phase, called the 'internal' wave. Typically the wave number of the 'external' wave is closer to the one of open water, named as the dominant wave mode for the two inviscid layers model. In addition there are infinitely many wave modes on the imaginary axis which are named evanescent waves. The mass loading model has only one propagating wave mode which corresponds to the 'external' wave. This is expected since the free surface and the interface in the mass loading model are always parallel. Figure 3 shows that the wave number from the mass loading

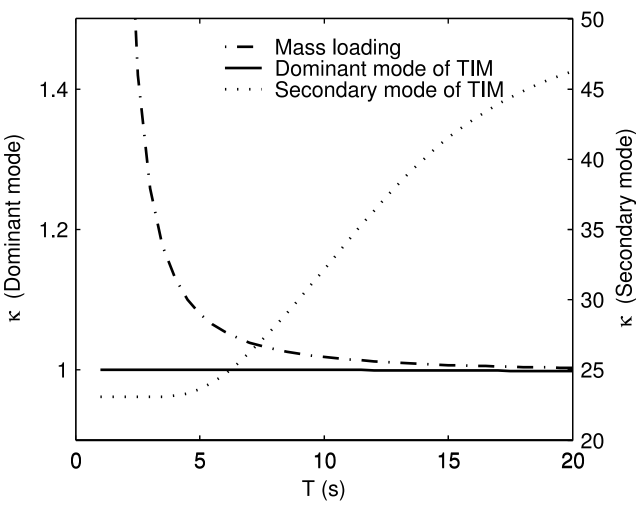

Figure 3. Comparison between mass loading model and two inviscid layers model (TIM). Parameters used are as follows: $h = 0.5\ m$, $H = 100\ m$.

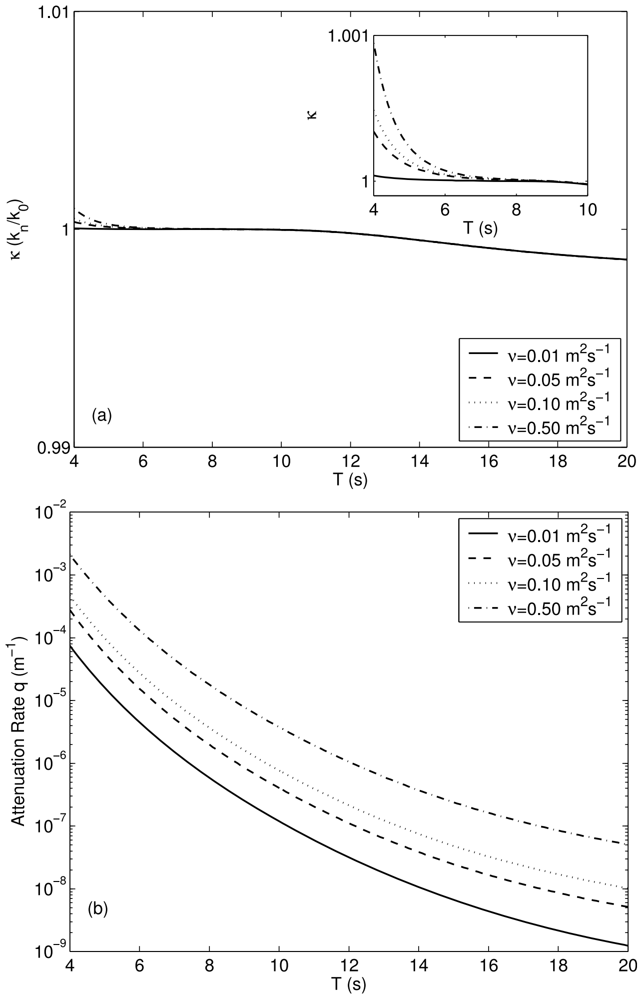

Figure 4. Viscous layer model for long waves. (a) Normalized wave number κ versus wave period $T(s)$ for the dominant wave mode and (b) attenuation rate $q(m^{-1})$ versus wave period $T(s)$ for the dominant wave mode. Parameters used are as follows: $h = 0.5\ m$, $H = 100\ m$, $G = 0$.

model converges to the dominant wave number from the two inviscid layers model as the wave period increases. This is because that for larger wave period which corresponds to $\tilde{k} \ll 1$, the mass loading model is the first order approximation of the two inviscid layers model, as shown in section 3. For a typical field case the two inviscid layers model predicts nearly no change in wave number when the wave propagates from open water to the ice-covered ocean. It implies that the two inviscid layers model is not applicable to describe the wavelength change observed in the field.

4.2. Viscous Layer Model

[24] When the viscosity of the ice layer is considered but the elasticity is ignored, such as one would expect from a frazil-grease ice cover, it is noted that many new wave modes appear in the four quadrants, and that the modes are antisymmetric. It is also found that the roots previously lined up along the imaginary axis rotate slightly about the origin if viscosity is considered.

[25] We shall only discuss our results in the intermediate to long wave regime (with period 4–20 s) which is typical in the field. In Figure 4, we present the wave number and wave attenuation rate of the dominant wave mode as the function of wave period for different viscosities. It is found that the wave number of the dominant wave mode is nearly the same as the one in open water for a wide range of wave periods and viscosities. However, the wave attenuation rate decreases with increasing wave period and increases with increasing viscosity. The ice thickness effect on the wave number and wave attenuation rate for different wave periods is plotted in Figure 5. It shows that the wave number of the dominant wave is almost independent of the ice thickness, and the wave attenuation rate increases with increasing ice thickness. It is also found that the wave attenuation rates of the secondary wave mode are several orders of magnitude larger than the one of the dominant wave mode, depending on the viscosity of the ice layer and the wave period. The secondary wave mode is defined as the one with the attenuation rate closest to the dominant wave mode.

4.3. Viscoelastic Model

[26] When both viscosity and elasticity are considered, the roots in the first quadrant rotate and tend to be symmetric as the elasticity increases. Figure 6 plots the typical behavior of

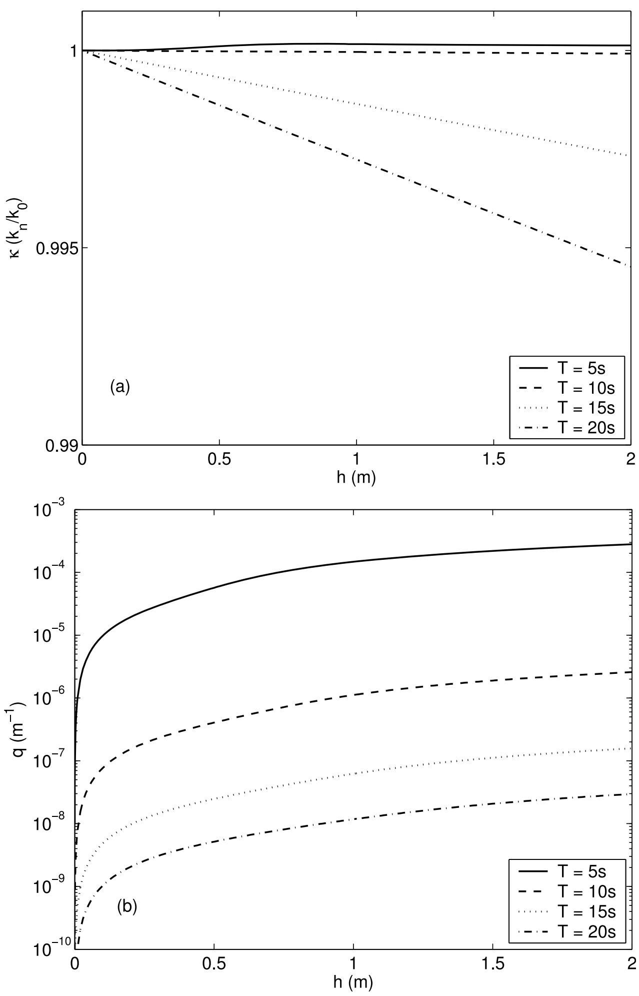

Figure 5. Ice thickness effect for viscous layer model. Parameters used are as follows: $H = 100\ m$, $\nu = 5 \times 10^{-2}\ m^2\ s^{-1}$, $G = 0$.

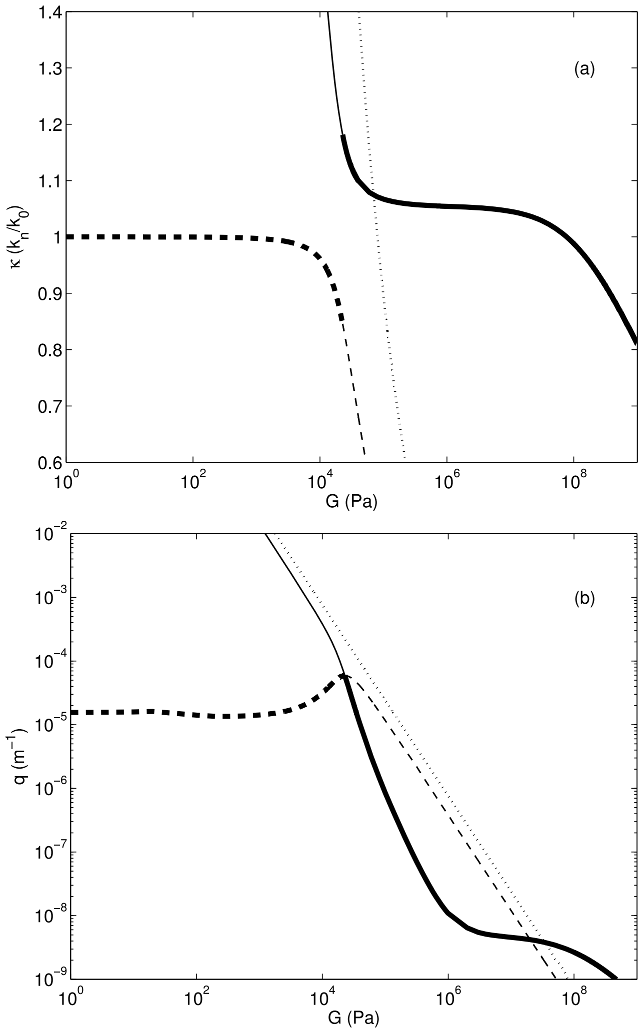

Figure 6. (a) Normalized wave number κ versus elasticity $G(Pa)$ and (b) attenuation rate $q(m^{-1})$ versus elasticity $G(Pa)$. Dashed curves represent the first mode, solid curves represent the second mode, and dotted curves represent the third mode. Heavy portions correspond to when the particular mode is dominant according to the two criteria. Note the switch of dominant mode between the first and the second. This switch occurs when the curves in Figure 6b cross. Parameters used are as follows: $h = 0.5\ m$, $H = 100\ m$, $\nu = 5 \times 10^{-2}\ m^2\ s^{-1}$, $T = 6\ s$.

the roots for (42) with respect to the elasticity parameter G. It shows that the first wave mode is dominant in the low elasticity regime, and it is very stable against variations of G when G is small. The second wave mode is dominant in the high elasticity regime and its wave number decreases with increasing elasticity. In the intermediate elasticity regime, when G is $10^4 \sim 10^5\ Pa$, the third wave mode approaches and departs k_0 rapidly. The approach of the third wave mode causes the other two wave modes to readjust their roles. The wave number from the first wave mode starts to move away from k_0 and the one from the second mode becomes closer to k_0. The attenuation rate of the first wave mode increases while that of the second decreases. At the crossing point the dominant wave mode switches from the first to the second. Thereafter, both the first and third wave modes approach zero wave number as G increases. This transitional behavior is observed in all cases analyzed. In the transition zone, all three wave modes could be physically important and form a complex wave packet. However, the third wave mode has a higher wave attenuation rate and only affects the transition zone, as shown in Figure 6. Beyond the transition zone, it is assumed that only one wave mode is dominant. In what follows we will focus on the dominant mode, either the first or the second mode depending on G.

[27] Figure 7 plots the wave number and wave attenuation rate of the dominant wave mode for various viscosity and elasticity. It shows that the dominant wave number is insensitive to viscosity regardless of the elasticity. The dominant wave attenuation rate increases as the viscosity increases. The behavior of the dominant wave mode as a function of the wave period is plotted in Figure 8. It shows that the wave number of the dominant wave mode is different from the one in open water only at smaller wave periods. The wave attenuation rate decreases as the wave period increases.

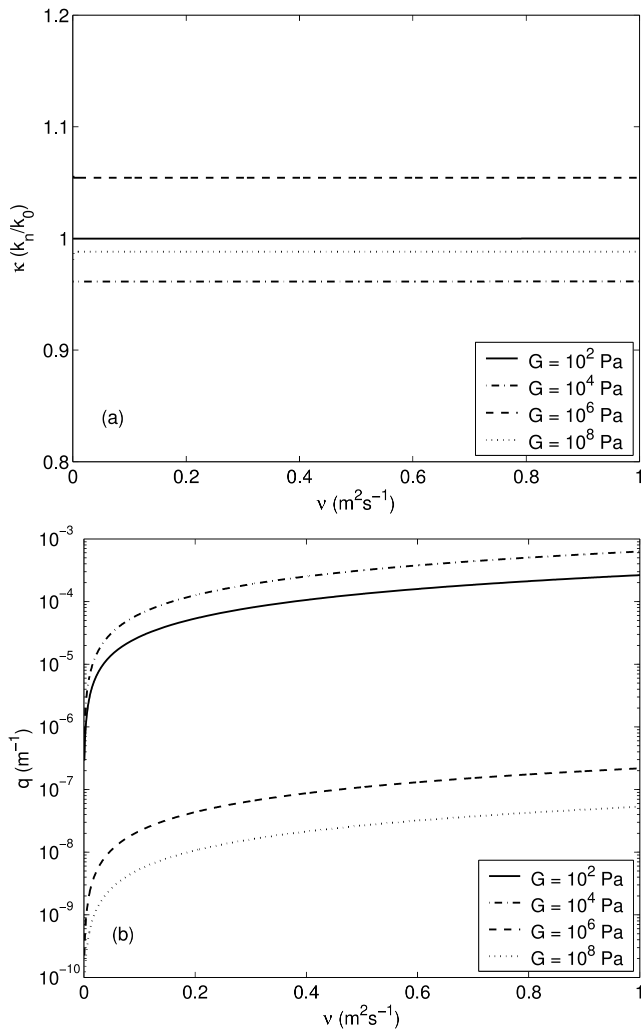

Figure 7. (a) Normalized wave number κ versus viscosity $\nu(m^2\ s^{-1})$ and (b) attenuation rate $q(m^{-1})$ versus viscosity $\nu(m^2\ s^{-1})$. Parameters used are as follows: $h = 0.5\ m$, $H = 100\ m$, $T = 6\ s$.

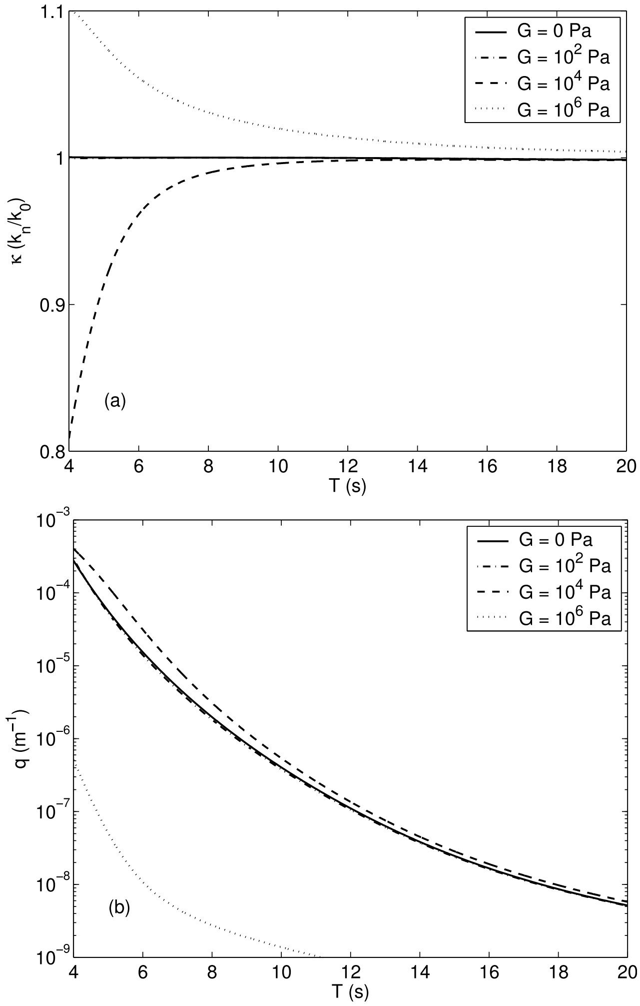

Figure 8. (a) Normalized wave number κ versus wave period $T(s)$ and (b) attenuation rate $q(m^{-1})$ versus wave period $T(s)$. Parameters used are as follows: $\nu = 5 \times 10^{-2}\ m^2\ s^{-1}$, $h = 0.5\ m$, $H = 100\ m$. All curves are for the dominant mode. For $G = 0$, 10^2, $10^4\ Pa$ this mode is the first one and for $G = 10^6\ Pa$ it is the second one.

4.4. Finite Elastic Plate Model and Thin Elastic Plate Model

[28] When viscosity is ignored and elasticity is considered, (44) becomes that of the finite elastic plate model. As discussed in section 3, the finite elastic plate model (FEPM) can be reduced to the widely used thin elastic plate model (TEPM) under the assumptions of long wave ($\tilde{k} \ll 1$) and large elasticity ($\rho\tilde{\sigma}^2/\tilde{G} \ll \tilde{k}^2$). Figure 9 plots the comparisons between FEPM and TEPM for ice thickness $h = 0.5\ m$ and $h = 3.0\ m$ with different wave periods. It shows that for large elasticity, the wave number from TEPM almost coincides with the dominant one from FEPM. For small elasticity, the wave number differences between TEPM and FEPM vary as wave period and ice thickness vary. The difference increases when the wave period decreases and the ice thickness increases. This is because smaller wave period and larger ice thickness correspond to a larger $\tilde{k}$, which violates the $\tilde{k} \ll 1$ requirement for TEPM. For a continuous ice sheet where the order of magnitude of elasticity is about $10^9\ Pa$, and $\rho\tilde{\sigma}^2/\tilde{G}$ is of order 10^{-7}, TEPM is a good approximation of FEPM. The fluctuation of κ in the dashed curve, as observed in Figure 9, results from the interaction of the second and the third mode as they approach each other. This fluctuation is more prominent when $\tilde{k}$ increases, i.e., when the wave period is low and the ice is thick. Incidentally, this fluctuation phenomenon is also present when viscosity is considered. The amplitude of fluctuation decreases with increasing viscosity. For a typical value of $\nu = 5 \times 10^{-2}\ m^2\ s^{-1}$, such as shown in Figure 6, the fluctuation is negligible.

5. Discussion

[29] In this study the ice-ocean system is modeled as a homogeneous viscoelastic ice layer of finite thickness overlying an inviscid water layer of finite depth. The visco-

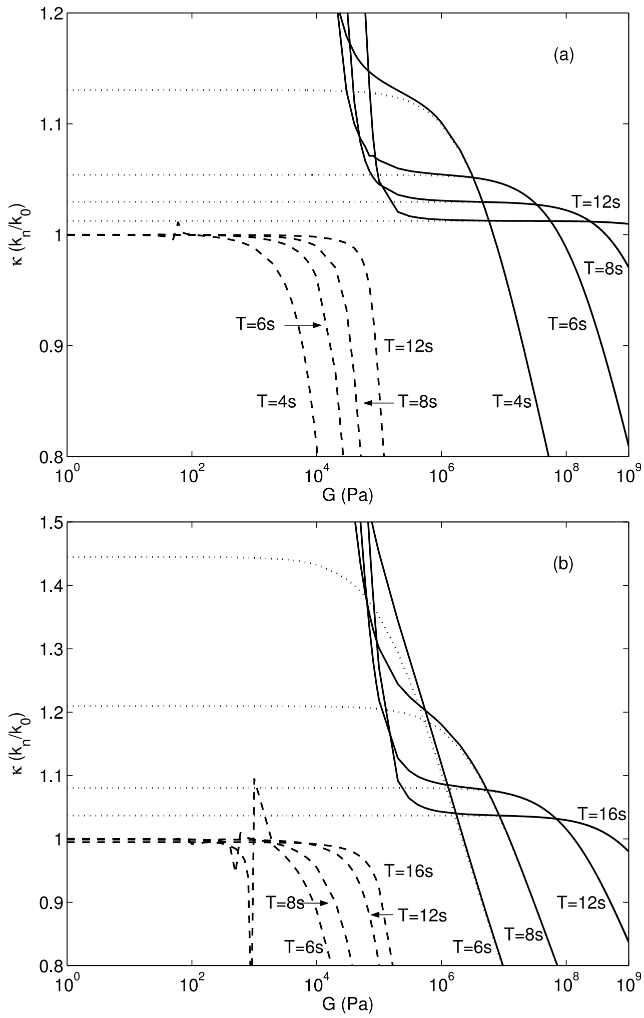

Figure 9. Comparisons between finite elastic plate model and thin elastic plate model for (a) $h = 0.5\ m$, $H = 100\ m$ and (b) $h = 3.0\ m$, $H = 100\ m$. Dotted curves represent the wave number from TEPM and dashed and solid curves represent the two wave modes from FEPM.

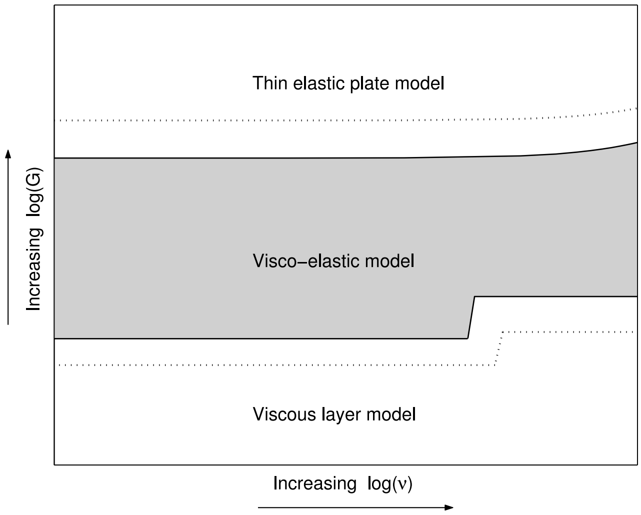

Figure 10. Zones of applicability for different models. The viscoelastic zone expands when kh increases, as shown by the dotted curves.

elastic property is represented by the Voigt model. The compact form of the resulting dispersion relation is obtained. The dispersion relation from the viscoelastic model covers those from several previously developed models.

[30] The viscoelastic model indicates that the open water wave splits into many wave modes when it propagates into the ice-covered ocean. However, only the wave mode most observable in the field is physically important, we name this mode as the dominant wave mode. Two criteria are used to select the dominant wave mode: (1) wave number is the closest to the open water value k_0 and (2) attenuation rate is the least among all modes. It is shown that there is always only one obvious wave mode, which is dominant in both small and large elasticity regimes regardless of the viscosity. In the intermediate elasticity regime, however, it appears that there are three wave modes with similar wavelengths and attenuation rates. Consequently, the criteria used to choose only one dominant wave mode may be insufficient to describe the wave characteristics accurately. In this case, the partition of wave energy into each of these three modes remains to be determined.

[31] In the small elasticity regime, the viscoelastic model predicts nearly no change in wave number ($\kappa \approx 1$) regardless of viscosity, wave period and ice thickness. In the large elasticity regime for a given ice thickness and wave period, there is a critical G_0. When $G < G_0$, waves shorten as they propagate into the ice cover. When $G > G_0$, waves lengthen. In this case, G_0 is independent of the viscosity. The wave attenuation rate depends on parameters such as ice thickness, wave period, the viscosity and the elasticity of an ice layer. In general, wave attenuation rate increases with increasing ice thickness and viscosity, and decreases with increasing wave period. The effect of elasticity on wave attenuation rate is very small when elasticity is small. As the elasticity increases, the wave attenuation rate starts to increase with elasticity until it reaches a maximum. At this point, the dominant wave mode switches and the attenuation begins to decrease with increasing elasticity. In the small elasticity regime, there are fluctuations appearing in a very small range of G. The fluctuation effect is significant for some extreme cases such as large kh and very small viscosity, which are not typically observed in the field. It can be concluded that this fluctuation will not affect the general conclusion discussed above. For large G, the thin elastic plate model is a good approximation to the finite thickness viscoelastic model; for small G, the results from viscous layer model are valid. Figure 10 summarizes the applicability of different models depending on the elasticity and viscosity of the ice field.

[32] Mechanisms controlling the interaction between waves and an ice cover depend on ice thickness, ice concentrations, ice temperature, and size distribution of ice floes. It is difficult to conduct field work and to parameterize this complicated process without a general model framework. From the above analysis two parameters, G and ν, are shown to control the wave-ice interaction. If we define λ as the ratio of ice floe size to wavelength, it is likely that the viscosity is a function of λ and the elasticity is a function of λ and ice temperature. When λ is very small, viscosity dominates and elasticity can be ignored. Viscosity can be determined by (44) through an inverse problem procedure: by measuring wave attenuation rate and ice thickness. When λ is large, elasticity dominates and the effect of viscosity becomes insignificant. Elasticity can be determined inversely by measuring wave number and ice thickness. When λ is in the intermediate range, all three parameters: wave number, wave attenuation rate, and ice thickness, should be measured to determine both viscosity and elasticity. Once the function between ice rheological parameters and λ is established, the wave characteristics in the whole ice field can be obtained from the viscoelastic model.

[33] The thickness of an ice cover can be determined by (42) for a given set of σ, H, G and ν. As shown in Figures 6 and 11, in the small elasticity regime, wave number is insensitive to h and G, but fortunately the attenuation rate is sensitive to ice thickness. Hence, the ice thickness can be determined by measuring the wave attenuation rate. In the large elasticity regime, the wave attenuation rate is too low to be measured, but the wave number is sensitive to the ice thickness. Ice thickness can be determined inversely by measuring the altered wave number. In the intermediate elasticity regime, both wave number and wave attenuation rate are sensitive to ice thickness so it can be determined by both the altered wave number and the attenuation rate.

[34] At $10^{-6}\ m^2\ s^{-1}$ the viscosity of water is four orders of magnitude lower than the reported ice viscosity and hence is not considered in this study. In our model, the wave decay mechanism is from the combination of viscosity and elasticity of ice layer only. In previous studies, eddy viscosity in the boundary layer under the ice cover was considered to describe the wave decay [*Weber*, 1987; *Liu and Mollo-Christensen*, 1988; *De Carolis and Desiderio*, 2002]. It is worth mentioning that if needed, the present approach can easily be extended to a more general model, in which the ice-ocean system can be treated as a viscoelastic ice layer overlying a viscous water layer. The only change would be to replace ice viscosity in De Carolis and Desiderio's model by the complex equivalent viscosity ν_e. However, this will introduce more parameters in the model and the eddy vis-

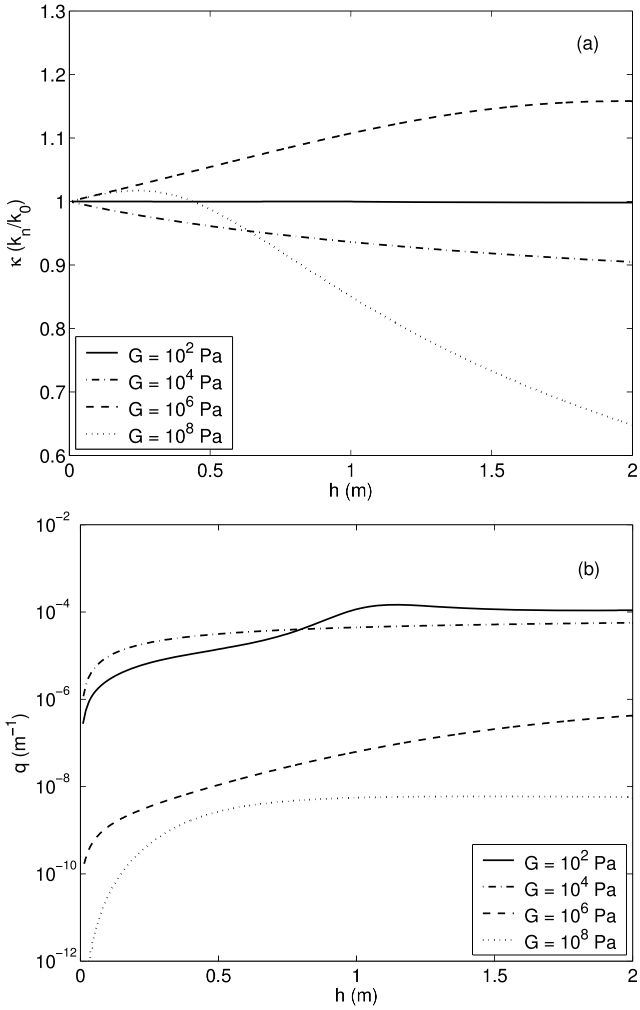

Figure 11. (a) Ice thickness effect on normalized wave number κ and (b) attenuation rate q from the viscoelastic model with different elasticity. Parameters used are as follows: $H = 100\ m$, $\nu = 5 \times 10^{-2}\ m^2\ s^{-1}$, $T = 6\ s$.

cosity is difficult to parameterize. In addition, a compact form of the dispersion relation may not be obtained easily.

6. Conclusion

[35] The viscoelastic constitutive law for an ice cover with finite thickness gives a general dispersion relation that can be reduced to previously established models. In this study we have found that there are several propagating modes under the ice cover. In most cases, only one mode is observable over a long distance. This mode coincides with those discussed in previous studies under various limiting conditions. For a range of intermediate elasticity, it appears that three equally dominant modes may coexist. These three wave modes, with similar wavelength and attenuation rate, can travel as a group. Implications of this intermediate range remain to be seen.

[36] There are two geophysical scale implications of the present study. The first concerns the ability for better forecasting ice conditions and the second concerns remote sensing of ice properties. We first consider forecasting. As the Arctic regions are becoming more dynamic and the desire for accurate ice predictions becomes more pressing, improved parameterization for different types of ice cover is needed. The long-term vision is that remote sensing and some sparse in situ data will be constantly collected to update the input parameters for a proper viscoelastic model. The model may then be used to simulate different types of ice cover based on: ice concentration, ice floe size distribution, and surface temperature. While realization of this prospect is still distant, the current study provides the necessary step to unify various theories for different types of ice cover. Second, the ability to determine the properties of ice cover is required for many offshore operations. Large scale survey of ice properties can only be done using satellites. The present study provides a tool to the inverse problem. If the ice type and wave properties are obtainable from satellites, the current theory gives a way to relate the dispersion and attenuation of the measured wave spectra to the ice thickness and the effective rigidity and viscosity. These three parameters are the key for many offshore applications such as navigation and structure designs.

[37] Currently our conjecture is that the two parameters: effective rigidity and viscosity are uniquely determined by the ratio of ice floe size to wavelength, ice concentration and ice temperature. Theoretical derivation of their relations is envisioned to be extremely challenging. Attempts to derive the viscosity of an idealized frazil ice layer [*De Carolis et al.*, 2005] exemplified the extent of this challenge. The most practical way to parameterize the rigidity and viscosity in the geophysical scale is through an inverse method, by simultaneously measuring ice and wave conditions in the field. We also envision carefully designed laboratory studies with controlled environment as an alternative to validate the viscoelastic model.

[38] **Acknowledgments.** The authors would like to thank Vernon Squire and the anonymous reviewers for comments that helped to improve this paper.

References

Balmforth, N. J., and R. V. Craster (1999), Ocean waves and ice sheets, *J. Fluid Mech.*, *395*, 89–124, doi:10.1017/S0022112099005145.
De Carolis, G., and D. Desiderio (2002), Dispersion and attenuation of gravity waves in ice: A two-layer viscous fluid model with experimental data validation, *Phys. Lett. A*, *305*, 399–412, doi:10.1016/S0375-9601(02)01503-7.
De Carolis, G., P. Olla, and L. Pignagnoli (2005), Effective viscosity of grease ice in linearized gravity waves, *J. Fluid Mech.*, *535*, 369–381, doi:10.1017/S002211200500474X.
Greenhill, A. G. (1886), Wave motion in hydrodynamics, *Am. J. Math.*, *9*, 62–112, doi:10.2307/2369499.
Keller, J. B. (1998), Gravity waves on ice-covered water, *J. Geophys. Res.*, *103*(C4), 7663–7669, doi:10.1029/97JC02966.
Lamb, S. H. (1932), *Hydrodynamics*, Dover, New York.
Liu, A. K., and E. Mollo-Christensen (1988), Wave propagation in a solid ice pack, *J. Phys. Oceanogr.*, *18*, 1702–1712, doi:10.1175/1520-0485(1988)018<1702:WPIASI>2.0.CO;2.
Liu, A. K., B. Holt, and P. W. Vachon (1991a), Wave propagation in the marginal ice zone: Model predictions and comparisons with buoy and synthetic aperture radar data, *J. Geophys. Res.*, *96*(C3), 4605–4621, doi:10.1029/90JC02267.
Liu, A. K., P. W. Vachon, and C. Y. Peng (1991b), Observation of wave refraction at an ice edge by synthetic aperture radar, *J. Geophys. Res.*, *96*(C3), 4803–4808, doi:10.1029/90JC02546.
Lu, P., Z. J. Li, Z. H. Zhang, and X. L. Dong (2008), Aerial observations of floe size distribution in the marginal ice zone of summer Prydz Bay, *J. Geophys. Res.*, *113*, C02011, doi:10.1029/2006JC003965.

Macpherson, H. (1980), The attenuation of water waves over a non-rigid bed, *J. Fluid Mech.*, *97*, 721–742, doi:10.1017/S0022112080002777.

Newyear, K., and S. Martin (1997), A comparison of theory and laboratory measurements of wave propagation and attenuation in grease ice, *J. Geophys. Res.*, *102*(C11), 25,091–25,099, doi:10.1029/97JC02091.

Newyear, K., and S. Martin (1999), Comparison of laboratory data with a viscous two-layer model of wave propagation in grease ice, *J. Geophys. Res.*, *104*(C4), 7837–7840, doi:10.1029/1999JC900002.

Ng, C. O., and X. Zhang (2007), Mass transport in water waves over a thin layer of soft viscoelastic mud, *J. Fluid Mech.*, *573*, 105–130, doi:10.1017/S0022112006003508.

Peters, A. S. (1950), The effect of a floating mat on water waves, *Commun. Pure Appl. Math.*, *3*, 319–354, doi:10.1002/cpa.3160030402.

Press, W. H., B. P. Flannery, S. A. Teukolsky, and W. T. Vetterling (1992), *Numerical Recipes: The Art of Scientific Computing*, Cambridge Univ. Press, New York.

Shen, H. H., S. F. Ackley, and M. A. Hopkins (2001), A conceptual model for pancake-ice formation in a wave field, *Ann. Glaciol.*, *33*, 361–367, doi:10.3189/172756401781818239.

Squire, V. A. (1984), A theoretical, laboratory, and field study of ice-coupled waves, *J. Geophys. Res.*, *89*(C5), 8069–8079, doi:10.1029/JC089iC05p08069.

Squire, V. A. (1993), A comparison of the mass-loading and elastic plate models of an ice field, *Cold Reg. Sci. Technol.*, *21*(3), 219–229, doi:10.1016/0165-232X(93)90066-H.

Squire, V. A. (2007), Of ocean waves and sea-ice revisited, *Cold Reg. Sci. Technol.*, *49*(2), 110–133, doi:10.1016/j.coldregions.2007.04.007.

Squire, V. A., and A. J. Allan (1980), Propagation of flexural gravity waves in sea ice, in *Sea Ice Processes and Models, Proceedings of the Arctic Ice Dynamics Joint Experiment*, edited by R. S. Pritchard, pp. 327–338, Univ. of Wash. Press, Seattle, Wash.

Squire, V. A., and C. Fox (1992), On ice-coupled waves: A comparison of data and theory, in *Advances in Ice Technology, Proceedings 3rd International Conference in Ice Technology*, edited by T. K. S. Murthy, W. M. Sackinger, and P. Wadhams, pp. 269–280, Comput. Mech., Wessex, U. K.

Squire, V. A., and S. C. Moore (1980), Direct measurement of the attenuation of ocean waves by pack ice, *Nature*, *283*, 365–368, doi:10.1038/283365a0.

Strathdee, J., W. H. Robinson, and E. M. Haines (1989), Moving loads on ice plates of finite thickness, report, Phys. and Eng. Lab., Lwer Hutt, N. Z.

Stroeve, J., M. Serreze, S. Drobot, S. Gearheard, M. Holland, J. Maslanik, W. Meier, and T. Scambos (2008), Arctic sea ice extent plummets in 2007, *Eos Trans. AGU*, *89*(2), 13–14, doi:10.1029/2008EO020001.

Wadhams, P. (1973), Attenuation of swell by sea ice, *J. Geophys. Res.*, *78*(18), 3552–3563, doi:10.1029/JC078i018p03552.

Wadhams, P., and M. J. Doble (2009), Sea ice thickness measurement using episodic infragravity waves from distant storms, *Cold Reg. Sci. Technol.*, *56*(2–3), 98–101, doi:10.1016/j.coldregions.2008.12.002.

Wadhams, P., and B. Holt (1991), Waves in frazil and pancake ice and their detection in Seasat synthetic aperture radar imagery, *J. Geophys. Res.*, *96*(C5), 8835–8852, doi:10.1029/91JC00457.

Wadhams, P., F. Parmiggiani, and G. De Carolis (2002), The use of SAR to measure ocean wave dispersion in frazil-pancake ice fields, *J. Phys. Oceanogr.*, *32*, 1721–1746, doi:10.1175/1520-0485(2002)032<1721:TUOSTM>2.0.CO;2.

Wadhams, P., F. F. Parmiggiani, G. de Carolis, D. Desiderio, and M. J. Doble (2004), SAR imaging of wave dispersion in Antarctic pancake ice and its use in measuring ice thickness, *Geophys. Res. Lett.*, *31*, L15305, doi:10.1029/2004GL020340.

Weber, J. E. (1987), Wave attenuation and wave drift in the marginal ice zone, *J. Phys. Oceanogr.*, *17*(12), 2351–2361, doi:10.1175/1520-0485(1987)017<2351:WAAWDI>2.0.CO;2.

Weitz, M., and J. B. Keller (1950), Reflection of water waves from floating ice in water of finite depth, *Commun. Pure Appl. Math.*, *3*, 305–318, doi:10.1002/cpa.3160030306.

H. H. Shen and R. Wang, Department of Civil and Environmental Engineering, Clarkson University, 8 Clarkson Ave., Potsdam, NY 13699, USA. (hhshen@clarkson.edu)